Compression theory for inhomogeneous systems

Doruk Efe Gökmen,[1] Sounak Biswas,[2] Sebastian D. Huber,[1] Zohar Ringel,[3] Felix Flicker,[4] and Maciej Koch-Janusz[5,6]

[1] *Institute for Theoretical Physics, ETH Zurich, 8093 Zurich, Switzerland*
[2] *Institut für Theoretische Physik und Astrophysik, Universität Würzburg, 97074 Würzburg, Germany*
[3] *Hebrew University, Racah Institute of Physics, Jerusalem, 9190401, Israel*
[4] *School of Physics and Astronomy, Cardiff University, Cardiff CF24 3AA, United Kingdom*
[5] *Department of Physics, University of Zurich, 8057 Zurich, Switzerland*
[6] *James Franck Institute, The University of Chicago, Chicago, Illinois 60637, USA*

The physics of complex systems stands to greatly benefit from the qualitative changes in data availability and advances in data-driven computational methods. Many of these systems can be represented by interacting degrees of freedom on inhomogeneous graphs. However, the irregularity of the graph structure and the vastness of configurational spaces present a fundamental challenge to theoretical tools, such as the renormalization group, which were so successful in characterizing the universal physical behaviour in critical phenomena. Here we show that compression theory allows to extract relevant degrees of freedom in arbitrary geometries, and develop efficient numerical tools to build an effective theory from data. We demonstrate our method by applying it to a strongly interacting system on an Ammann-Beenker quasicrystal, where it discovers an exotic critical point with broken conformal symmetry.

Introduction – Dramatic improvements in data availability, stemming from both experiments and simulation, enable the exploration of increasingly complex physical systems. A glut of raw data does not, however, equate understanding, particularly when its processing easily exceeds our computational resources. A key objective is to distill data into a succinct theory in terms of appropriate collective variables that uncovers and summarizes the essence of the system. Renormalization Group (RG) approaches in statistical physics provide a systematic path towards that goal [1, 2]. However, both identifying the relevant degrees of freedom (DOFs), as well as executing the mathematical procedure deriving the effective theory [3, 4] is often extremely challenging in inhomogeneous systems when prior intuition is scarce.

Many complex systems are, alas, inhomogeneous, or even owe their properties precisely to the lack of translation invariance. Problems as disparate as biological tissue mechanics [5–7] and properties of metallic glasses [8, 9] can be cast as statistical mechanical problems on irregular graphs. We would like to understand the emergent behaviour of such systems much in the same fashion RG has allowed us to understand critical phenomena in translationally invariant systems.

Here we tackle the two challenges of inhomogeneity and vast configurational spaces of complex systems. Formulating the RG of an inhomogeneous system as a lossy compression of information [10, 11] on a graph allows us to define the procedure in a manner that is independent of geometry. We develop efficient numerical tools based on contrastive learning to perform it on high-dimensional data [12–14].

Our algorithm explicitly constructs new effective DOFs $\mathcal{H}^i$ on a local subgraph $\mathcal{V}^i$. This is achieved by a coarse graining transformation $\mathbf{\Lambda}^i$ *locally* chosen in region i to maximise the following mutual information [15–17]

$$\arg\max I(\mathcal{H}^i : \mathcal{E}^i) = \mathbf{\Lambda}^i : \quad \mathcal{V}^i \mapsto \mathcal{H}^i, \tag{1}$$

where the environment $\mathcal{E}^i$ is defined using the graph distance (Fig. 1).

The variational principle in Eq. 1 provides a powerful substitute for intuition: effective DOFs are individually designed by the statistics of their *local* environment. This is essential for moving beyond translation invariance. While the coarse graining $\mathbf{\Lambda}^i$ erases microscopic fluctuations, its local optimisation in turn allows to retain the distinct qualitative characteristics that emerge in different spatial regions across an inhomogeneous system. This can even be reflected in a non-uniform cardinality of compressed variables $\mathcal{H}^i$, as illustrated in Fig. 1.

We illustrate the power of this approach by constructively proving an open conjecture regarding the presence of discrete scale invariance (DSI) [18–20] of a strongly correlated statistical model on a quasicrystal [21]. We explicitly construct macroscopic variables self-similar to the microscopic ones, and perfectly compatible with the hierarchical structure of the quasiperiodic tiling. Our graph-based tool leverages the computational backend of the RSMI-NE package [15, 22], allowing for efficient exploration of the large-scale behavior of the model.

The system – The Ammann-Beenker (AB) construction gives quasiperiodic tilings of the plane utilizing two distinct plaquettes: a rhombus and a square [23]. Like their famous cousins, the Penrose tilings [24], AB tilings feature diffraction patterns exhibiting crystallographically "forbidden" symmetries, here 8-fold [25]. Likewise, they can also be generated by a recursive procedure in which an *inflation* map σ acts on a small seed patch by decomposing the constituent plaquettes as shown in Fig. 2b, and subsequently rescaling all the edge lengths by the silver ratio $\delta = 1 + \sqrt{2}$. A special role is played by 8-fold coordinated vertices: under inflations all lower coordinated vertices ultimately become (and stay) 8-vertices. Each 8-vertex is characterised by an *order*, *i.e.* the maximal number of inverse *deflations* σ^{-1} after

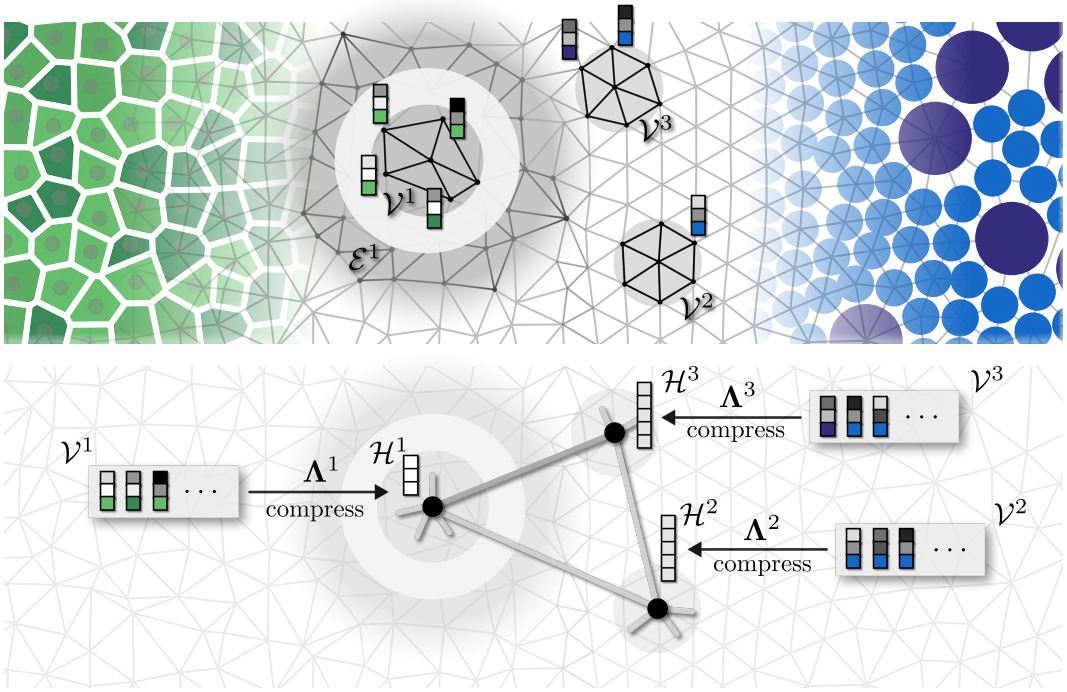

FIG. 1. Constructing effective degrees of freedom in inhomogeneous systems. Distinct systems like tissues (left, in green) and colloidal suspensions (right, in blue) can be abstracted into a set of vector degrees of freedom $\mathcal{V}^i$ (here shown by rectangles, and $i = 1, 2, 3$) living on an irregular graph with local structure. The final component of the vectors are shown by coloured boxes to indicate different types of degrees of freedom, unique to each system. To derive a compressed representation of such systems, it is essential to tailor the coarse graining transformation $\mathbf{\Lambda}^i$ for each local neighbourhood i. This is achieved by an information theoretic variational principle, where $\mathbf{\Lambda}^i : \mathcal{V}^i \mapsto \mathcal{H}^i$ maximises the mutual information $I\left(\mathcal{H}^i : \mathcal{E}^i\right)$. This allows the compressed variables $\mathcal{H}^i$ to capture the emergent long-range physics according to the statistics of surrounding distant environment $\mathcal{E}^i$. Local optimisation can produce compressed variables with varying cardinality across the system, here illustrated by vectors $\mathcal{H}^i$ of varying number of components. Finally, the connectivity of the emergent supergraph is determined through the correlations of the new variables.

which it still remains 8-fold coordinated. The order of an 8-vertex intuitively specifies the maximal size of the local patch centered on it, within which the lattice appears perfectly 8-fold symmetric. The quasiperiodic AB lattice is thus invariant under discrete rescalings. Such discrete rescalings are easily visualized for even order deflations σ^{2n} by drawing a super-lattice connecting 8-fold vertices (Fig. 2a).

Dimer models enjoy a deceptively simple definition: the microscopic dimers live on the links of (any) lattice, which can be either occupied or empty. The key element is a set of hard local constraints: at every vertex where the links meet, one and only one of the links is occupied. This gives rise to a surprisingly rich phenomenology. Dimer models on regular lattices have been studied extensively, in part due to their relevance to high-T_c superconductivity [26], but have since been shown to support topological order and fractionalisation [27, 28] and exotic critical points [29]. The classical version is closely related to the quantum one [30, 31] and has deep connections to combinatorics [32–34] and the study of random surfaces [35, 36].

Recent work has begun to explore the interplay of (strongly-correlated) dimer physics and quasiperiodicity. Particularly, AB tilings, in contrast to Penrose tilings [37], host perfectly matched dimer configurations in the thermodynamic limit (*i.e.* with a vanishing density of defects), and numerically computed dimer correlations exhibit a quasi power-law decay with a complex spatial structure [21]. Moreover, the combinatorial proof of perfect matching pointed to a hierarchy of self-similar effective matching problems at different scales.

Taken together these facts suggest a conjecture that not only the AB tilings themselves, but crucially also the *physics* of the dimers on the AB tilings, exhibit DSI [21] – a potentially striking and unusual example of the relevance of quasiperiodicity for the critical behaviour. A proof, and a microscopic physical mechanism at the level of the dimer ensemble was, however, absent. The putative criticality naturally calls for a RG analysis, but general RG approaches for quasiperiodic systems in $D \geq 2$ dimensions are in their infancy.

Results – We address, in turn, two key questions using our compression approach based on Eq. 1: what are the local effective DOFs, and what is the structure of their correlations. This is systematically revealed by the

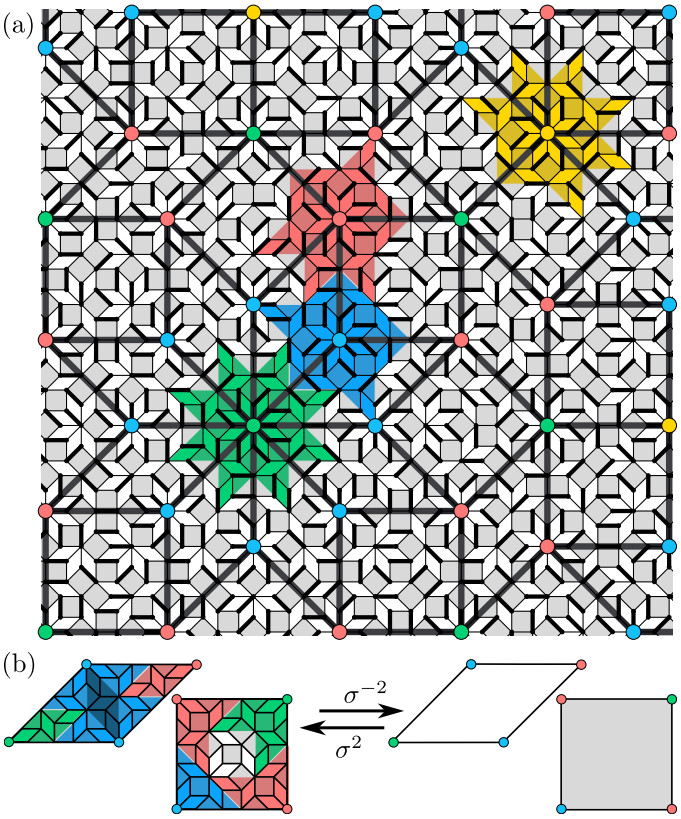

FIG. 2. Self-similarity of the Ammann-Beenker tiling, and the coarse graining blocks. (a) A microscopic dimer configuration (small black links) on the AB tiling's edges, with an overlaid AB *superlattice*, self-similar to the microscopic one. The effective DOF at a supervertex of a given (colour coded) valence will be obtained by coarse graining the dimer configuration in the surrounding region $\mathcal{V}$ of a shape dictated by the inflation rules and shown as a polygon of a matching colour. (b) The inflation (deflation) $\sigma^{2(-2)}$ of the elementary rhombi and squares generating the tiling, with parts of the polygonal domains indicated in colour. Coarse graining all such polygonal patches executes a deflation σ^{-2} of the original AB lattice, yielding the superlattice shown.

analysis of data provided by our algorithm.

To uncover the emergent DOFs, we need to specify the spatial partition for the blocks $\mathcal{V}$ first. In the AB tiling there are natural choices, set by the recursive structure of the AB lattice itself [38]. At each scale, the AB tiling can be covered by four "classes" of blocks [21], shown in Fig. 2 in different colours, each deflating to vertices of differing connectivity in the super-lattice.

In each inequivalent class, the algorithm identifies the emergent DOF as a $\mathbb{Z}_n$ *clock variable*, with n the connectivity, or class, of $\mathcal{V}$ in the superlattice. This is revealed as follows: the variational compression map $\mathbf{\Lambda}$ assigns to a Monte Carlo dimer configuration $\mathcal{V}$ a short binary code $\mathcal{H}$ (Fig. 3a), the bits being set by applying individual components Λ_k to $\mathcal{V}$ (itself a long bitstring of dimer occupations in the block). Each component of the vector $\mathbf{\Lambda}$ is *a priori* a general nonlinear map, parametrized by a neural network, whose output is finally binarized.

The length of the code is *not* supplied, but found by sequentially increasing the number of components in $\mathbf{\Lambda}$, and training the compression of $\mathcal{V}$ to optimally preserve the mutual information with its environment $\mathcal{E}$. Crucially, the maximal retained information about $\mathcal{E}$ plateaus with the optimal code-length *depending on the class* of block region $\mathcal{V}$. Particularly, for $\mathcal{V}$ in class-8 the optimal number of components is four, while for class-3 only two (Fig. 3b,f). Further, nonlinearity of $\mathbf{\Lambda}$ networks does not improve compression: the same amount of information is preserved with only linear components. Optimal linear maps on the space of dimer configurations on V are shown for classes 8 and 3 in Figs.3c and g, respectively.

To unravel the physical content of these encodings, we further query the outputs of our algorithm. The code statistics in Fig. 3d reveal striking features: of the sixteen 4-bit codes in class-8 only eight are ever assigned, with half of the codes unused. Yet in Fig. 3b a 3-bit encoding, which has exactly eight available codes, is suboptimal. Moreover, the frequencies of all class-8 codes used are the same (Fig. 3d), while for class-3 only two frequencies are identical (Fig. 3h). These puzzling results indicate that the optimal compression finds structure beyond merely the number of states of the DOF, which is essential to correlations with $\mathcal{E}$, and which *cannot* be encoded with fewer bits.

We thus investigate the codes, and the $\mathbf{\Lambda}$ maps. We first note that the 4-bit codes form a closed 8-cycle, with neighbours differing by a single bit-flip, and each code having exactly two 1-bit distant neighbours (Fig. 3e) [39]. The uniform frequencies and the cyclic structure of the code hint at a symmetry.

Indeed, a class-8 patch $\mathcal{V}$ of the AB *lattice* is locally symmetric under $\pi/4$ rotations. We observe that under such rotations the components of the optimal $\mathbf{\Lambda}$ map in Fig. 3c change as

$$\mathsf{C}_8: \quad (\Lambda_1, \Lambda_2, \Lambda_3, \Lambda_4) \to (\Lambda_4, -\Lambda_3, -\Lambda_1, -\Lambda_2), \qquad (2)$$

which is a representation of a generator of the cyclic group C_8. We emphasize that it is the compression map, and consequently the emergent DOF now carrying a representation of what is *a priori* a (local) symmetry only of the AB lattice.

Similar analysis can be performed for other classes of $\mathcal{V}$, which have a mirror symmetry. In particular, under its action for the class-3 patch in Fig. 3g we have

$$\text{mirror}: \quad (\Lambda_1, \Lambda_2) \to (\Lambda_2, \Lambda_1), \qquad (3)$$

explaining equal frequency of the **01** and **10** codes. Hence, we conclude that, rather than becoming continuous, the emergent DOFs of the dimer system at σ^2 scale remain discrete, and mimic the local symmetry of the underlying super-lattice. This holds equally at σ^4 scale, providing the first indication of DSI.

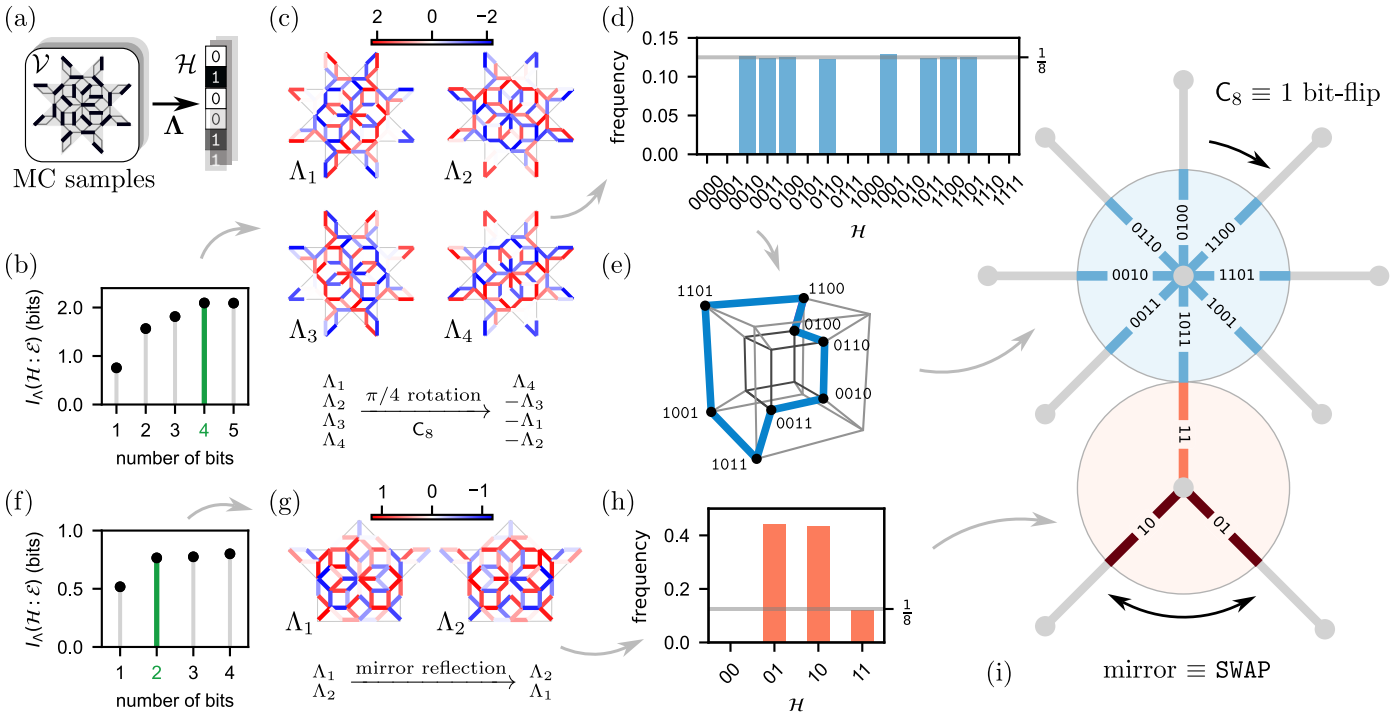

FIG. 3. Finding effective clock variables. (a) Coarse graining transformation $\mathbf{\Lambda}$ mapping Monte Carlo configurations on $\mathcal{V}$ into bitstrings $\mathcal{H}$ on supervertices of σ^{-2} deflated tiling. (b, f) The length of the bitstring $\mathcal{H}^{8(3)}$ is determined by the saturation of mutual information at 4 (2) bits at 8 (3)-supervertices. Each bit $\mathcal{H}_k$ is decided by the sign of the linear transformation $\Lambda_k \cdot \mathcal{V}$. The respective optimal filters $\mathbf{\Lambda}$ in (c, g) carry a representation of the local spatial symmetries of corresponding supervertices, namely C_8 and mirror. (d, h) The probability distributions $P(\mathcal{H}^{8(3)})$ occupy the space of codes sparsely, and form abstract clock variables. (e) In particular, $\mathcal{H}^8$ forms a closed 8-loop, where each state has exactly two neighbours with Hamming-distance 1. (i) The representations of the local symmetries on filters induce transitions between adjacent clock-states, enabling to identify abstract clock-states with spatial directions along the links of the quasiperiodic lattice (see main text).

Having found the emergent DOFs in each class $\mathcal{V}$ individually, we turn to their correlations, where DSI manifests itself fully. To this end we simultaneously coarse grain dimer configurations in multiple blocks, which collectively form an AB superlattice as in Fig. 2a, using the trained compression maps (Fig. 3c,g).

As noted before, the number of states of each emergent DOF equals the connectivity of the supervertex it lives on. Since the distribution of each state's frequencies reflects the underlying superlattice symmetry, these internal DOFs can be identified with spatial orientations along the edges of the superlattice. For example, since mirror symmetry w.r.t. the axis connecting the 8- and 3-vertices in Fig. 3i relates the code frequencies of the 3-vertex codes **01** and **10** (Fig. 3h), the remaining state **11** is the one pointing towards the 8-vertex.

We probe the correlations by conditioning on the state of one of the vertices. In Fig. 4b,c, fragments of σ^{-2} and σ^{-4} superlattices are shown, with the state of the conditioning variable, identified with a direction, in orange, while the conditional distribution of DOFs at the other vertices in greyscale. Remarkably, this distribution is very strongly correlated, effectively forcing occupation of some states, and excluding others. To wit, when the 3-vertex DOF points towards the 8-vertex, the distribution $P(\mathcal{H}|\mathcal{H}^3)$ of the latter is sharply peaked in the matching direction, while *no other neighbour* of the 3-vertex points towards it (allowing, for example, the identification of the 8-vertex code **1011** with a spatial orientation in Fig. 3i). Conversely, when the 3-vertex DOF points towards one of its other neighbours, it is "matched" by the latter, while the 8-vertex DOF distribution has zero weight *precisely and only* in the direction towards that 3-vertex.

Examining all such correlations we arrive at a striking conclusion: the effective DOFs in $\mathcal{V}$'s throughout the lattice are paired with *one and only one* of their neighbours into emergent "super-dimers" on the edges of the superlattice. The exclusion of certain clock variable orientations in Figs. 3a-e is a precise reflection of the hard dimer-constraints, which these super-dimers obey. Moreover, comparison of further correlations to those of the microscopic dimers in Fig. 4a reveals that not just the local-dimer constraints, but also longer-range correlations are reproduced correctly. The physics of the microscopic dimer model on the AB lattice is thus replicated to a high degree of accuracy at the δ^2 scale and, again, at the δ^4 scale (where "locking" is even sharper, see Fig. 4c), thereby demonstrating DSI across three scales.

The quasiperiodicity of the AB lattice and the strong interactions of the dimer model conspire to *re*create self-

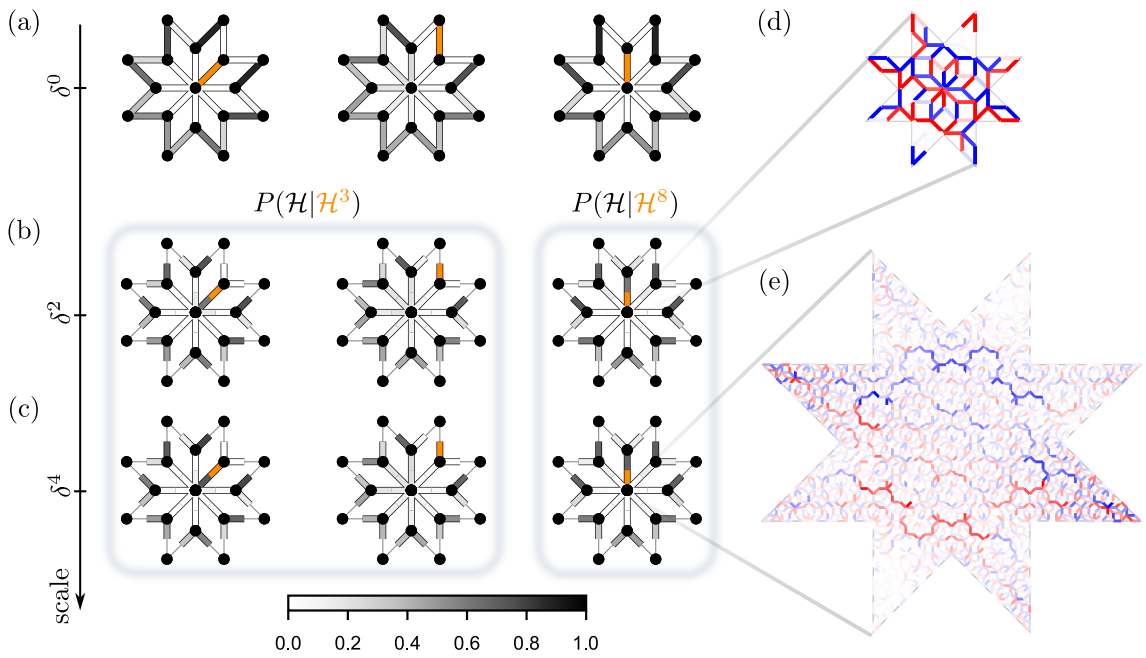

FIG. 4. Emergent dimer exclusion rule and self-similar dimer-dimer correlations across scales. (a) The probability distribution of microscopic (*i.e.* δ^0) dimers (in greyscale) on an AB patch, conditioned on one of the links (in orange) hosting a dimer. (b, c) First two columns: the probabilities $P(\mathcal{H}|\mathcal{H}^3)$ of the *emergent* clock variables on the δ^2 and δ^4 superlattice (in greyscale), conditioned on two distinct states of one of the 3-clocks (in orange). The third column shows distributions conditioned on a state of the central 8-clock. Binding of adjacent clock variables into super-dimers obeying dimer exclusion constraints is revealed by sharply peaked conditional distributions. The effective super-dimers reproduce also longer-range dimer-dimer correlations at both δ^2 and δ^4 scales. (d, e) Examples of (a single component of) optimal coarse-graining filters producing the central 8-state clock variable at scales δ^2 and δ^4. The latter comprises 2760 microscopic links.

similar DOFs at a higher scale, giving rise to DSI, which we uncover guided by the outputs of our algorithm A parallel work [40] gives a microscopic interpretation of these emergent super-dimers as alternating dimer paths with respect to a certain reference configuration, and studies the criticality numerically.

We emphasize the dual computational and conceptual aspect of this result: each compression map $\mathbf{\Lambda}$ at the σ^4 scale is a highly structured function of approximately 10^3 microscopic dimer occupations ($\sim 2^{10^3}$ configurations), effectively impossible to guess or analyze by hand only, and yet providing sharp and concise physical insights about DOFs, symmetries, and correlations. We have, in effect, reached a point where ML techniques can not only assist, but facilitate progress in theoretical physics.

Our results demonstrate that using lossy compression effective DOFs and their theory can be extracted from the structure of information inherent in raw high-dimensional data, and that this approach excels in systems with irregular geometry. These characteristics are essential in e.g. complex biological sytems and in disordered materials.

Acknowledgements – D.E.G., and S.D.H. gratefully acknowledge financial support from the Swiss National Science Foundation. S.B. acknowledges support by the European Research Council under the European Union Horizon 2020 Research and Innovation Programme via Grant Agreement No. 804213-TMCS. Z.R. acknowledges support from ISF grant 2250/19. M.K.-J. gratefully acknowledges financial support from the European Union's Horizon 2020 programme under Marie Sklodowska-Curie Grant Agreement No. 896004 (COMPLEX ML).

[1] Kenneth G. Wilson, "Renormalization Group and Critical Phenomena. I. Renormalization Group and the Kadanoff Scaling Picture," Phys. Rev. B **4**, 3174–3183 (1971).
[2] Leo P. Kadanoff, "Scaling laws for ising models near T_c," Phys. Phys. Fiz. **2**, 263–272 (1966).
[3] Shang-keng Ma, Chandan Dasgupta, and Chin-kun Hu, "Random antiferromagnetic chain," Phys. Rev. Lett. **43**, 1434–1437 (1979).
[4] Ferenc Iglói and Cécile Monthus, "Strong disorder rg approach of random systems," Physics Reports **412**, 277–431 (2005).

[5] Alexander G. Fletcher, Miriam Osterfield, Ruth E. Baker, and Stanislav Y. Shvartsman, "Vertex models of epithelial morphogenesis," Biophysical Journal **106**, 2291–2304 (2014).

[6] Silvanus Alt, Poulami Ganguly, and Guillaume Salbreux, "Vertex models: from cell mechanics to tissue morphogenesis," Philosophical Transactions of the Royal Society B: Biological Sciences **372**, 20150520 (2017).

[7] Reza Farhadifar, Jens-Christian Röper, Benoit Aigouy, Suzanne Eaton, and Frank Jülicher, "The influence of cell mechanics, cell-cell interactions, and proliferation on epithelial packing," Current Biology **17**, 2095–2104 (2007).

[8] J. D. Bernal, "Geometry of the structure of monatomic liquids," Nature **185**, 68–70 (1960).

[9] H. Sheng, W. Luo, F. Alamgir, J. Bai, and E. Ma, "Atomic packing and short-to-medium-range order in metallic glasses," Nature 10.1038/nature04421.

[10] N. Tishby, F. C. Pereira, and W. Bialek, "The information bottleneck method," in *Proceedings of the 37th Allerton Conference on Communication, Control and Computation*, Vol. 49 (2001).

[11] Amit Gordon, Aditya Banerjee, Maciej Koch-Janusz, and Zohar Ringel, "Relevance in the renormalization group and in information theory," Phys. Rev. Lett. **126**, 240601 (2021).

[12] Mohamed Ishmael Belghazi, Aristide Baratin, Sai Rajeshwar, Sherjil Ozair, Yoshua Bengio, Aaron Courville, and Devon Hjelm, "Mutual information neural estimation," *Proceedings of the 35th International Conference on Machine Learning*, Proceedings of Machine Learning Research, **80**, 531–540 (2018).

[13] Ben Poole, Sherjil Ozair, Aaron Van Den Oord, Alex Alemi, and George Tucker, "On variational bounds of mutual information," in *Proceedings of the 36th International Conference on Machine Learning*, Proceedings of Machine Learning Research, Vol. 97, edited by Kamalika Chaudhuri and Ruslan Salakhutdinov (PMLR, 2019) pp. 5171–5180.

[14] Aaron van den Oord, Yazhe Li, and Oriol Vinyals, "Representation learning with contrastive predictive coding," (2019), arXiv:1807.03748 [cs.LG].

[15] Doruk Efe Gökmen, Zohar Ringel, Sebastian D. Huber, and Maciej Koch-Janusz, "Statistical physics through the lens of real-space mutual information," Phys. Rev. Lett. **127**, 240603 (2021).

[16] Patrick M. Lenggenhager, Doruk Efe Gökmen, Zohar Ringel, Sebastian D. Huber, and Maciej Koch-Janusz, "Optimal renormalization group transformation from information theory," Phys. Rev. X **10**, 011037 (2020).

[17] Maciej Koch-Janusz and Zohar Ringel, "Mutual information, neural networks and the renormalization group," Nature Physics **14**, 578–582 (2018).

[18] Didier Sornette, "Discrete-scale invariance and complex dimensions," Physics reports **297**, 239–270 (1998).

[19] Jeremy T. Young, Alexey V. Gorshkov, Michael Foss-Feig, and Mohammad F. Maghrebi, "Nonequilibrium fixed points of coupled ising models," Phys. Rev. X **10**, 011039 (2020).

[20] Grace M. Sommers, Michael J. Gullans, and David A. Huse, "Self-dual quasiperiodic percolation," Phys. Rev. E **107**, 024137 (2023).

[21] Jerome Lloyd, Sounak Biswas, Steven H. Simon, S.A. Parameswaran, and Felix Flicker, "Statistical mechanics of dimers on quasiperiodic Ammann-Beenker tilings," Phys. Rev. B **106** (2022).

[22] Doruk Efe Gökmen, Zohar Ringel, Sebastian D. Huber, and Maciej Koch-Janusz, "Symmetries and phase diagrams with real-space mutual information neural estimation," Phys. Rev. E **104**, 064106 (2021).

[23] B. Grunbaum and G.C. Shephard, *Tilings and Patterns* (W. H. Freeman and Company, 1986).

[24] R. Penrose, "The role of aesthetics in pure and applied mathematical research," Bull. Inst. Math. Appl. **10**, 266–271 (1974).

[25] Marjorie Senechal, *Quasicrystals and Geometry* (Cambridge University Press, 1996).

[26] Daniel S. Rokhsar and Steven A. Kivelson, "Superconductivity and the quantum hard-core dimer gas," Phys. Rev. Lett. **61**, 2376–2379 (1988).

[27] R. Moessner and S. L. Sondhi, "Resonating Valence Bond Phase in the Triangular Lattice Quantum Dimer Model," Phys. Rev. Lett. **86**, 1881–1884 (2001).

[28] R. Moessner, S. L. Sondhi, and Eduardo Fradkin, "Short-ranged resonating valence bond physics, quantum dimer models, and ising gauge theories," Phys. Rev. B **65**, 024504 (2001).

[29] T. Senthil, Ashvin Vishwanath, Leon Balents, Subir Sachdev, and Matthew P. A. Fisher, "Deconfined quantum critical points," Science **303**, 1490–1494 (2004).

[30] Fabien Alet, Jesper Lykke Jacobsen, Grégoire Misguich, Vincent Pasquier, Frédéric Mila, and Matthias Troyer, "Interacting Classical Dimers on the Square Lattice," Phys. Rev. Lett. **94**, 235702 (2005).

[31] Fabien Alet, Yacine Ikhlef, Jesper Lykke Jacobsen, Grégoire Misguich, and Vincent Pasquier, "Classical dimers with aligning interactions on the square lattice," Phys. Rev. E **74**, 041124 (2006).

[32] Richard Kenyon and Andrei Okounkov, "What is a dimer?" Notices of the AMS **52** (2005).

[33] P.W. Kasteleyn, "The statistics of dimers on a lattice: I. The number of dimer arrangements on a quadratic lattice," Physica **27**, 1209–1225 (1961).

[34] Henry Cohn, Richard Kenyon, and James Propp, "A variational principle for domino tilings," Journal of the American Mathematical Society **14**, 297–346 (2001).

[35] Richard Kenyon, Andrei Okounkov, and Scott Sheffield, "Dimers and amoebae," Annals of Mathematics **163**, 1019–1056 (2006).

[36] Richard Kenyon and Andrei Okounkov, "Limit shapes and the complex Burgers equation," Acta.Math. **199**, 263–303 (2007).

[37] Felix Flicker, Steven H. Simon, and S.A. Parameswaran, "Classical Dimers on Penrose Tilings," Phys. Rev. X **10** (2020).

[38] A. Jagannathan, "Quantum spins and quasiperiodicity: A real space renormalization group approach," Phys. Rev. Lett. **92**, 047202 (2004).

[39] Interestingly, this solves the four dimensional 'coil in the box' problem familiar from coding theory.

[40] Sounak Biswas and S. A. Parameswaran, "Discrete scale invariant fixed point in a quasiperiodic classical dimer model," (2023).

[41] NetworkX developers, "NetworkX: Network Analysis in Python," (2014-2023).

[42] Doruk Efe Gökmen, Zohar Ringel, Sebastian D. Huber, and Maciej Koch-Janusz, "RSMI-NE/RSMI-NE," (2021-2023).

Supplemental materials

Appendix A: Methods

a. Real-space mutual information based coarse-graining – The method used to construct the effective degrees of freedom (DOFs) is a generalisation of the compression theoretic approach first introduced by some of the authors in [17] in translation invariant systems. The key insight is that the random variables, such as the coarse-grained area $\mathcal{V}$ and the environment $\mathcal{E}$, in variational principle in Eq. 1 can be defined in any metric space, and are not restricted to regular lattices. Here we use the graph distance which provides a meaningful measure for spatial length scale on graphs with a local structure.

The second issue that the above construction solves is that the coarse-grained lattice structure is defined by the correlations of the emergent DOFs themselves. Dealing with the changing coarse-grained lattice is the main problem in RG approaches on disordered systems [4]. Taken together, these two properties indicate that the approach defined by Eq. 1 provides a mathematical definition of coarse graining valid in inhomogeneous systems with local structure.

In concrete terms, the procedure is defined as follows. Consider a system of microscopic DOFs is described by a (large dimensional) random variable $\mathcal{X}$ distributed according to some joint probability distribution $P(\mathcal{X})$. A coarse-graining (CG) of a partition $\mathcal{X} = \bigcup_i \mathcal{V}^i$ into new variables $\mathcal{X}' = \bigcup_i \mathcal{H}^i$ is then defined as a conditional probability distribution $P(\mathcal{X}'|\mathcal{X}) = \prod_i P_{\mathbf{\Lambda}^i}(\mathcal{H}^i|\mathcal{V}^i)$ where $\mathcal{X}' = \bigcup_i \mathcal{H}^i$ and where the product is over individual CG of a blocks variables $\mathcal{V}^i \mapsto \mathcal{H}^i$. We emphasise there is a distinction between the spatial patch V, and a configurations of DOFs supported on it this patch (a random variable) $\mathcal{V}$, which we glossed over in the main text. The correct meaning is implied by the context. The patch V can be chosen as any local subgraph, for instance a topological ball defined using graph distance, or another set dictated by the structure of the problem, such as the tiles we used in the AB example (Fig. 2a).

Maximisation of the real-space mutual information (RSMI)

$$I_{\mathbf{\Lambda}^i}(\mathcal{H}^i : \mathcal{E}^i) = \mathbb{E}_{(\mathcal{H}^i,\mathcal{E}^i)}\left[\log P(\mathcal{H}^i,\mathcal{E}^i) - \log P(\mathcal{H}^i)P(\mathcal{E}^i)\right]$$

between $\mathcal{H}^i$ and its distant environment $\mathcal{E}^i$ provides a variational principle for the CG map $\mathbf{\Lambda}^i$ to distill the most relevant long-range features [11, 16]. The compression is enforced by limiting the information capacity of $\mathcal{H}^i$ using a predetermined number of encoding bits, thereby providing an approximation to the information bottleneck problem [11].

This computationally difficult variational principle *can* nevertheless be efficiently implemented with differentiable parametric lower bounds on mutual information. Such bounds are parametrised by a deep NN, and optimised simultaneously with the parameters $\mathbf{\Lambda}^i$ of the coarse-graining using stochastic gradient descent. This is the RSMI-NE algorithm, which some of the authors introduced recently [15, 22].

Here we extended this formalism and the RSMI-NE package to systems on arbitrary static graphs by casting the configurations into vectors according to the fixed coordinate system defined by the graph. The new graph-enabled RSMI-NE code using the NetworkX backend [41] is available publicly [42].

b. Ansatz – We parametrised the coarse graining $P_{\mathbf{\Lambda}^i}(\mathcal{H}^i|\mathcal{V}^i)$ with an inner-product ansatz $\mathcal{H}^i_k := \text{sign}\left(\mathbf{\Lambda}^i_{kj}\mathcal{V}^i_j\right)$, parametrised by a vector of linear NNs $\mathbf{\Lambda}^i = (\Lambda^i_k)$. The index k runs over the components of a coarse-grained variable, and the index j refers to the spatial positions in region $\mathcal{V}$, where the indexing is defined with respect to a fixed labelling of vertices in the graph. Though we considered scalar DOFs in the original system, vector DOFs $\mathcal{V}^i_{jl}$ can also be handled by increasing the rank of the coarse grainer by one: Λ^i_{kjl}. Our code supports also more general mappings that do not have this multilinear structrure, and are instead parametrised by general NNs.

For mapping binary variables we used annealed Gumbel-softmax reparametrisation with exponential relaxation rate 5×10^{-3}. The critic function in the variational RSMI lower-bound is implemented using a separable architecture

$$f(\mathcal{H}, \mathcal{E}) = u(\mathcal{H})^{\mathrm{T}} v(\mathcal{E})$$

where u and v are two-layer deep NNs with hidden dimension 16 and output dimension 8 (the latter is contracted in the inner product of the two networks).

We trained the neural networks using stochastic gradient descent with learning rate 10^{-3} using 50000 sample dimer configurations, generated via the directed-loop Monte Carlo algorithm on the AB graph indicated with the gray links in Fig. S2 (containing 26177 nodes). The sample dataset is supplied to the RSMI-NE algorithm in minibatches of size 1000 and 120 epochs of the entire dataset.

The coarse-grained block variable $\mathcal{V}$ at a given scale δ^n is defined on the σ^n inflated tiles V shown with different colours in Fig. 2a. The environment regions E, are defined as a shell with radius given by a fixed graph-distance from the centre of V. In particular for δ^2, E is defined by an inner radius $L_{E_\text{i}} = 9$ and outer radius $L_{E_\text{o}} = 24$, whereas for δ^4 we used $L_{E_\text{i}} = 40$, $L_{E_\text{o}} = 64$, as shown in Fig. S1. In Fig. S2 we show examples of corresponding σ^{-4} coarse-graining filters optimised for these regions.

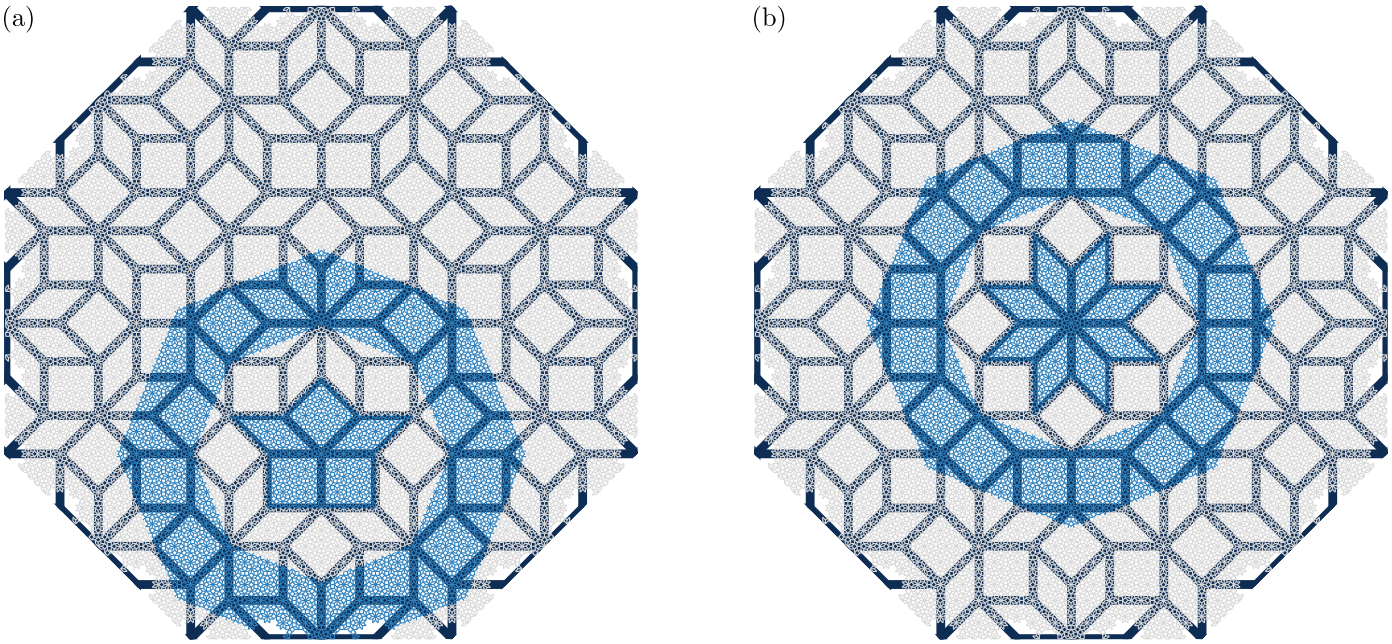

FIG. S1. Block and environment regions. Highlighted in blue are examples of the coarse-graining blocks V, and their annular environment regions E used for the 3- (a) and 8-vertices (b) at the largest scale considered (*i.e.* δ^4). The microscopic lattice, and the σ^{-2} superlattice are shown. The centers of the "kite" and "star" shaped regions V are at the 8-vertices whose positions form the σ^{-4} superlattice.

Appendix B: The odd scales

Our analysis of the coarse graining transformations of the dimer model on the AB tiling *did not* find evidence for a discrete scale invariant description in terms of super-dimer variables under all rescalings, but only for *even* order ones (*i.e.* under deflations σ^{-2k}). This is in contrast to the AB tiling itself (*i.e.* just the AB lattice), which is invariant under any order of deflation.

In addition, our method finds quantitatively and qualitatively distinct behaviour at odd orders σ^{-1} and σ^{-3}. The maximal mutual information $I_\Lambda(\mathcal{H}:\mathcal{E})$ attained for the coarse graining at a 3-supervertex is non-monotonic, exhibiting, within error, two distinct values characterizing the even and odd scales (with the odd scales' information reduced to almost half), as shown in Fig. S3.

Furthermore, the optimised coarse graining does not yield a well-defined three-state clock variable at odd scales. Indeed, for even scales the optimisation robustly yields a well-defined set of three clusters (corresponding to the three clock states) even in the distribution of pre-activations $\mathbf{\Lambda} \cdot \mathcal{V}$, while at odd scales the distribution of pre-activations lacks any such clear structure. We emphasize that this is *not* an optimization issue: computationally, σ^{-4} coarse graining is a more challenging problem than σ^{-3} (because of much large size of random variables involved).

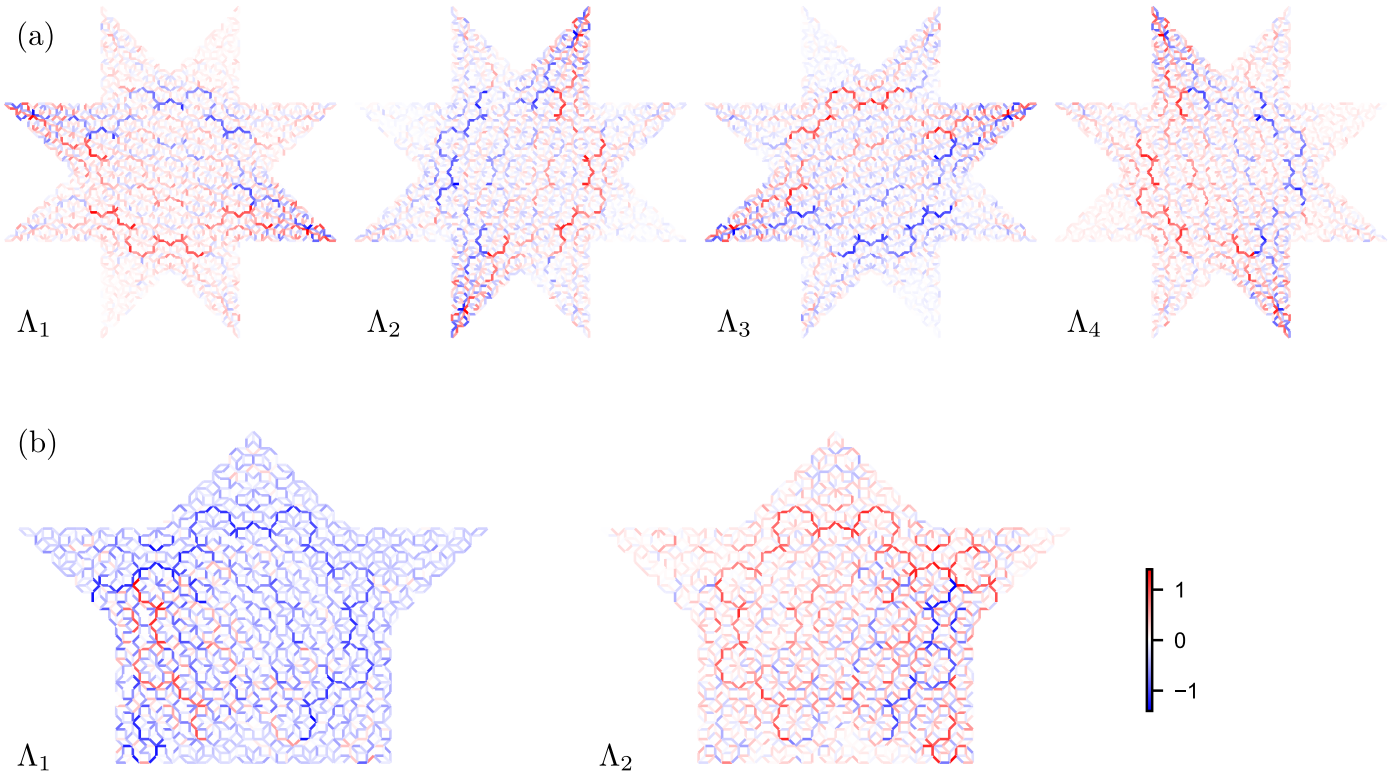

FIG. S2. Optimal σ^{-4} coarse-graining transformations. (a) 8-supervertex filters. (b) 3-supervertex filters.

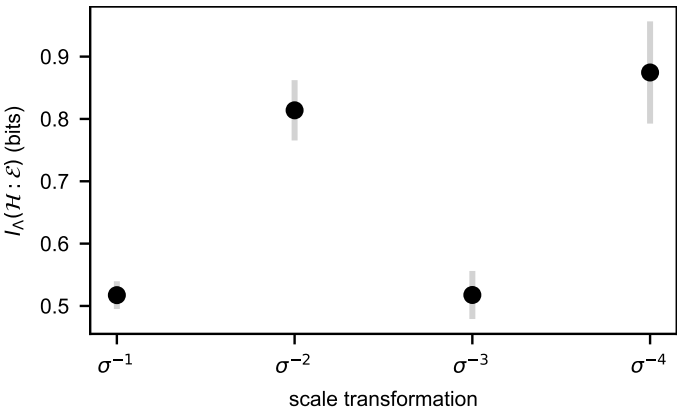

FIG. S3. Mutual information across different scale transformations. The maximal MI for the coarse graining at a 3-supervertex. For odd order rescaling transformations $\sigma^{-1,-3}$, the information attained by the compression is systematically lower compared to the even ones $\sigma^{-2,-4}$.